IUST
Iran University of Science and Technology

Iranian Journal of Electrical and Electronic Engineering

Journal Homepage: ijeee.iust.ac.ir

Torque Ripple Mitigation and Fault-Tolerant Operation of Modular Twelve-Phase PMSM Drive using Model-Free Predictive Control

Davood Maleki* and Abolfazl Halvaei Niasar *(C.A.)

Abstract: In electric propulsion systems for high-power applications, multi-phase Permanent Magnet Synchronous Motors (PMSMs) are highly advantageous due to their fast dynamic response and high reliability. This study investigates a twelve-phase PMSM with double stator windings, where each winding is powered by a single-phase H-bridge inverter. The control of both H-bridge inverters for each phase is managed by a dedicated microcontroller. Given the independence of the control systems (microcontrollers) and the absence of data exchange between them, the modeling is conducted in the 12-phase stationary reference frame. To address non-sinusoidal back-EMF phase voltages and mitigate torque ripple, a harmonic current injection method is independently applied to each phase. A model-free predictive current and speed controller (MFPCSC), based on an ultra-local model, is employed, replacing conventional PI or hysteresis current controllers. Additionally, extended state observers (ESOs) are designed to estimate uncertainties and parameter mismatches. Under fault conditions, a fault-tolerant control strategy is implemented, where the current angle of healthy windings is adjusted to suppress the second harmonic in the remaining healthy windings, thereby reducing torque ripple. The effectiveness of the proposed control methods is validated through simulations, both under normal operating conditions and various fault scenarios.

Keywords: PMSM Drive, 12-phase double winding, H-bridge inverter, reliability, model-free predictive control, fault-tolerant control.

1 Introduction

In electric drives used for special applications, high reliability is a critical design requirement. To achieve this, suitable motors, qualified components, and robust hardware and software are essential. For instance, hardware design strategies may include redundancy measures such as increasing the number of motor phases, adding extra switches, using independent single-phase inverters (e.g., H-bridge for each phase), redundant control systems and microcontrollers, and redundant sensors. Additionally, fault-tolerant control (FTC) methods enable the drive to continue operating without significant disruption in the event of a failure [1]. Permanent magnet synchronous motors (PMSMs) are particularly attractive for electric drives due to their high power and torque density, smooth torque output, high efficiency, and reliability. However, despite the inherent reliability of three-phase PMSMs with star-connected windings, a fault in one inverter switch or winding can cause the motor to stop producing torque. To enhance reliability—especially in high-power applications—multi-phase PMSMs are increasingly used in vessels and submarine vehicles. Increasing the number of phases reduces the phase current, mitigating motor losses and cooling challenges [2].

For low- to medium-power applications, three-phase PMSMs with double-star windings (asymmetric six-phase) are common, while twelve-phase PMSMs are preferred for high-power applications. Multi-phase

Iranian Journal of Electrical & Electronic Engineering, 2026.
Paper first received 13 Feb. 2025 and accepted 14 Jul. 2025.
* The author is with the Department of Electrical & Computer Engineering, University of Kashan, Kashan, Iran.
E-mail: d.maleki1391@gmail.com
E-mail: halvaei@kashanu.ac.ir.
Corresponding Author: Abolfazl Halvaei Niasar.

PMSMs can be categorized into two types: symmetrical and asymmetrical. Symmetrical multi-phase PMSMs, such as five-phase and seven-phase motors, typically have an odd number of phases. Asymmetrical multi-phase PMSMs, on the other hand, consist of multiple sets of three-phase windings (e.g., six-phase or twelve-phase). In asymmetrical PMSMs with N sets (N = 2, 3, ...) of three-phase windings, the angle (β) between identical windings in different sets is "$\pi/3N$". These motors offer higher reliability than symmetrical multi-phase PMSMs, as each three-phase set can be powered by an independent three-phase inverter. Fig. 1(a) illustrates a twelve-phase PMSM with individual single-phase inverters [3]. Fig. 1(b) shows a twelve-phase PMSM with four three-phase windings (each with a separate star point) powered by four independent three-phase inverters. Scheme (b) is the traditional drive design for a twelve-phase PMSM, that the motor has four symmetrical three-phase winding sets, with the corresponding windings in the three different phases having a spatial distance of 15 degrees. Fig. 2 shows the schematic of the drive system of twelve-phase PMSM [4] of Scheme (b). Fig. 1(a) has the highest level of reliability because, each phase of the motor is powered separately from an independent single-phase H-bridge inverter, and in the event of a fault in one winding or in one H-bridge inverter, the remaining 11 phases of the motor continue to develop torque [6]. This topology is designed and implemented in a modular manner. The features of this design include the high number of switches, which is 48, which is twice the number of switches in Fig 2.

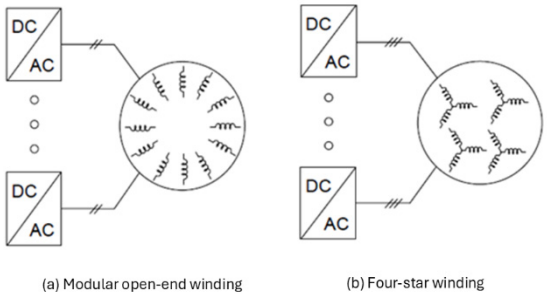

Fig 1. Common types of electrical drives for 12-phase PMSM [3]

To enhance the performance of a PMSM drive under fault conditions, it is essential to first identify the source and location of the fault and then apply an appropriate control strategy [5]. Drive faults can be broadly classified into two categories: mechanical faults and electrical faults. Electrical faults account for more than 90% of drive failures, making fault-tolerant control primarily focused on addressing these faults. Electrical faults can be further categorized into five types: Inverter faults, Stator faults, Sensor faults, Control system faults, and Magnet demagnetization faults.

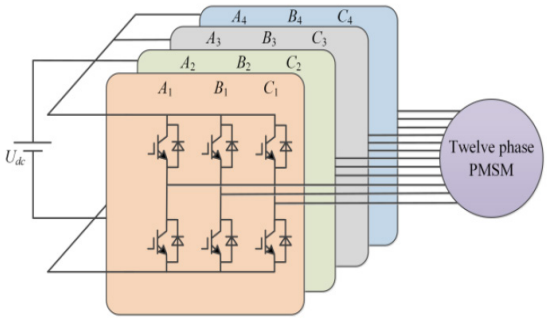

Fig 2. Circuit diagram of a twelve-phase PMSM driven by four separate three-phase inverters [4]

Among these, inverter faults are the most common [6]. Fault-tolerant control in PMSM drives typically employs a combination of software and hardware methods. The software approach involves modifying the control strategy after a fault occurs, while the hardware approach usually entails using a fault-tolerant inverter topology instead of a conventional inverter to ensure uninterrupted operation. Ideally, integrating both methods yields the most effective fault-tolerant control solution.

This work utilizes a modular topology (similar to Fig. 1(a)) with the highest reliability. The system consists of a twelve-phase PMSM with double windings, where each motor phase is split into two windings producing the same magnetomotive force (MMF). As illustrated in Fig. 3, the phase windings are distributed at 15-degree intervals.

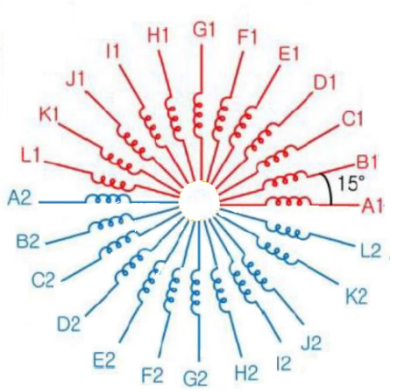

Fig 3. Stator winding configuration of a 12-phase PMSM with dual windings

Each half of a phase winding is placed 180 degrees apart on the stator circumference, ensuring exact alignment between the two halves. Notably, this motor employs 24 independent single-phase H-bridge inverters with a total of 96 switches, controlled by 12 separate microcontrollers. Fig. 4 depicts the modular drive schematic for the double-winding, twelve-phase PMSM, where each half-winding is powered by a dedicated H-

bridge inverter. The two inverters corresponding to a single phase are commended by a local microcontroller, which operates independently without data exchange with other controllers. A central microcontroller provides the phase current reference. Due to the complete independence of the microcontrollers, conventional modeling, estimation, and control methods based on multiple dq-reference frame theory are not applicable in this configuration.

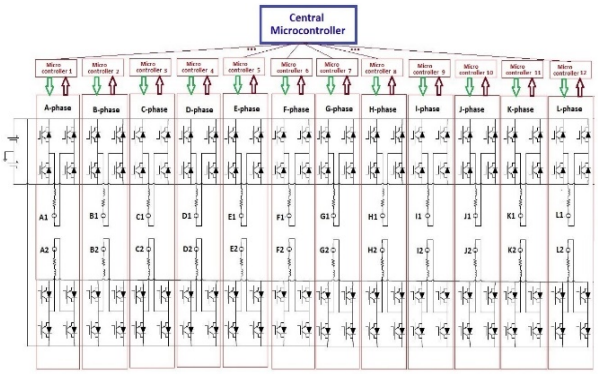

Fig 4. Schematic diagram of the modular drive system for the twelve-phase PMSM with dual windings proposed in this study

2 Modeling of modular twelve-phase PMSM motor with double winding

Sinusoidal three-phase PMSMs are typically modeled in the two-axis dq rotating reference frame and controlled using field-oriented control (FOC). Similarly, for twelve-phase PMSMs, three primary modeling approaches exist:

1. Separate Modeling of Four Three-Phase Groups – Each group is modeled in its own dq reference frame [7].
2. Decoupled Modeling of Four Three-Phase Groups – The groups are decoupled but modeled in a single dq reference frame [8].
3. Vector Space Decomposition (VSD) Modeling – A more generalized approach that decomposes harmonics [9].

However, the modular drive system used in this study (Fig. 4) employs local microcontrollers for each phase group, which operate independently without intercommunication. Consequently, dq-based modeling methods (such as Park transformations) are unsuitable. Additionally, if the PMSM's back-EMF contains non-sinusoidal harmonics, Park transformations fail to accurately represent motor behavior. Several alternative modeling methods for non-sinusoidal PMSMs have been proposed:

1. Extended Park Transform [10]
2. dq Modeling with Harmonic Compensation [11]
3. Multiple Rotating Frame (MRF) Modeling [12]
4. Vector Space Decomposition (VSD) [13]

While these methods are effective for three-phase PMSMs, they impose a high computational burden—especially when scaled to twelve-phase systems. Among them, VSD is the most suitable for non-sinusoidal twelve-phase PMSMs. However, VSD and other dq-based methods require a centralized controller, whereas the modular drive system in this study distributes control across local microcontrollers. Since these microcontrollers cannot perform 3-to-2 transformations (or vice versa), dq-frame modeling is infeasible. For a twelve-phase PMSM with non-sinusoidal back-EMF and modular control, modeling must instead be performed in a twelve-axis stationary reference frame, where adjacent windings are spaced 15 electrical degrees apart (Fig. 3).

This approach is viable for surface-mounted PMSMs, where self- and mutual inductances remain constant. Assuming the phase winding arrangement in Fig. 3, the voltage-current relationship for each winding follows:

$$v_x = R_s i_x + \frac{d}{dt}\psi_x + e_x \tag{1}$$

where, R_s is the resistance of each winding, and v_x, i_x, ψ_x and e_x represent the voltage, current, flux linkage and back-EMF voltage due to the rotor flux of the xth winding, respectively, that $x = A_1, A_2, B_1, B_2, \dots, L_2$. The flux linkage of each winding depends on its own current as well as the current of the other 23 windings, and can be calculated as follows:

$$\psi_x = L_x i_x + \sum_{\substack{y=A_1,A_2,B_1,B_2,\dots,L_2 \\ (x\neq y)}} M_{xy} i_y \tag{2}$$

Here, L_x is the self-inductance of winding x and M_{xy} is the mutual inductance between the windings x and y. The electromagnetic torque (T_e) and the mechanical speed (ω_m) of the double twelve-phase motor can be calculated using the following relations:

$$T_e = \sum_{x=A_1,\dots,L_2} \frac{e_x i_x}{\omega_r} \tag{3}$$

$$\omega_m = \frac{1}{J}\int (T_e - B\omega_m - T_L)dt \tag{4}$$

where, ω_r, J, B and T_L are the rotor electrical speed, the total moment of inertia of the rotor, friction coefficient and the load torque, respectively. To implement the motor model in Simulink, a 24-phase winding can be used, where, each winding is connected in series with a

speed-dependent voltage source e_x. The waveform of e_x may contain arbitrary harmonics and depends on the rotor position θ_r.

3 Control of modular twelve-phase PMSM using harmonic current injection strategy and MFPCSCs

Various control methods exist for three-phase PMSMs, many of which can theoretically be extended to twelve-phase PMSM motors. However, due to the increased phase count, computational complexity, microcontroller processing limitations, and the suboptimal performance of some methods in high-power applications, their practical implementation remains limited [14]. Among the available techniques, field-oriented control (FOC) in the dq reference frame is the most widely adopted method for twelve-phase PMSMs. This approach is essentially an extension of the three-phase PMSM control strategy. Several variations of FOC have been proposed in the literature for twelve-phase PMSMs. In [15], the reference values for the d- and q-axis current components are derived based on the sinusoidal nature of the back-EMF voltages. Ref. [15] employs a distributed vector control method, similar to [15], where each three-phase stator group is independently controlled in its own dq reference frame using PI controllers. To mitigate magnetic coupling effects between groups, decoupling voltage signals are injected into the current controller outputs. Ref. [16] presents a vector control strategy based on the VSD (Vector Space Decomposition) model. Here, the 12-phase currents are transformed into two subspaces: the dq plane (for fundamental torque production) and the harmonic subspace (z_1z_2). PI and PR controllers are then applied to suppress harmonic current components. Ref. [17] extends the dq-frame vector control approach to a dual twelve-phase PMSM, demonstrating its applicability in more complex multi-phase systems.

Apart from the vector control method, model predictive control (MPC) is also employed for twelve-phase PMSM drives. Increasing the number of phases significantly expands the number of available voltage vectors. For instance, in [18], only 24 effective voltage vectors are selected from 4,096 possible candidates to evaluate the cost function in the proposed finite-control-set MPC (FCS-MPC) scheme. FCS-MPC utilizes the motor's mathematical model to predict the control effort and then optimizes the cost function to minimize the error between the predicted and reference values [19-20]. However, during motor operation, parameter variations—caused by factors such as temperature fluctuations and magnetic saturation—degrade the controller's accuracy, leading to compromised performance in both transient and steady-state conditions. To address this issue, several solutions have been proposed. In [21], a model-independent control strategy is introduced, leveraging an ultra-local model to compensate for parameter variations, inverter nonlinearities, and mutual coupling effects. This approach incorporates parameter identification to estimate system disturbances. A model-free predictive current control (MFPCC) method for PMSM drives is presented in [22]. In [23], an MFPCC scheme based on a nonlinear disturbance observer (NDO) is proposed. Here, parameter variations are treated as disturbances, and the control strategy relies on disturbance estimation to maintain robustness.

Most conventional control methods rely on the motor model in the two-axis dq reference frame, necessitating the use of Park or Clarke transformations. However, in the modular drive structure of this study—where each phase's control system operates independently without knowledge of the other phases—these traditional methods are not applicable. To enhance the robustness of the PMSM drive system against disturbances and parameter variations, this study proposes a model-free predictive control (MFPC) method. The key innovation lies in the simultaneous current and speed control using a model-free approach, augmented by a nonlinear disturbance observer (NDO) to maintain robustness under motor parameter changes. By integrating these features and eliminating the PI speed controller, the proposed method improves reliability in tracking reference values within a defined transient period. The developed model-free predictive current and speed control (MFPCSC), combined with the NDO, is also applicable to non-sinusoidal PMSMs, effectively minimizing torque ripple and reducing acoustic noise. To further mitigate torque ripple caused by high-order harmonics in the phase back-EMF voltages, this study employs a harmonic current injection method (reference current shaping) in the 12-axis stationary reference frame. A brief explanation of this technique follows.

3.1 Torque control using harmonic current injection method

In the harmonic current injection method, harmonic currents are injected into each phase to compensate for the harmonics present in the back-EMF voltage. The amplitudes of these injected currents are adjusted such that the harmonic components of the torque are canceled out, leaving only a constant torque [14,25].

For the motor studied in this study, it is assumed that only the 1st, 3rd, 5th, and 7th harmonics are present in the back-EMF voltages. Thus, the back-EMF voltage of winding x $(x = A_1, A_2, B_1, B_2, \dots, L_2)$ can be expressed as follows:

$$e_x(t) = E_1 \sin \omega_r t + E_3 \sin 3\,\omega_r t + E_5 \sin 5\,\omega_r t + E_7 \sin 7\,\omega_r t \quad (here;\ x = A_1 \text{ or } A_2) \tag{5}$$

Here E_1 to E_7 represent the harmonic amplitudes of the back-EMF voltages, which in this study are set to 1, 0.2, 0.1, and 0.02 per unit, respectively. If the current injected into coil x is defined as follows:

$$i_x(t) = I_1 \sin \omega_r t + I_5 \sin 5\,\omega_r t + I_7 \sin 7\,\omega_r t \quad (6)$$

The air gap power of winding x will only include even harmonics up to order 14th and will be as follows:

$$P_x(t) = P_0 + P_2 \sin 2\omega_r t + \cdots + P_{14} \sin 14\,\omega_r t \quad (7)$$

It can be analytically demonstrated that in a PMSM with a phase number that is a multiple of 3, the air-gap power (or torque)—comprising the sum of contributions from all windings—contains only harmonic components of orders that are multiples of 6. For the motor under study in this study, by restricting the harmonic analysis to the 7th order, the instantaneous air-gap power P_e is derived as follows:

$$P_e(t) = P_0 + P_6 \sin 6\omega_r t + P_{12} \sin 12\,\omega_r t \quad (8)$$

And the instantaneous electromagnetic torque can also be calculated as follows:

$$T_e(t) = \frac{P_e(t)}{\omega_r} = T_0 + T_6 \sin 6\omega_r t + T_{12} \sin 12\,\omega_r t \quad (9)$$

where:

$$T_0 = \frac{3}{2\omega_r}[\ E_1, E_5, E_7\ ] \quad (10)$$

$$T_6 = \frac{3}{2\omega_r}[I_1(E_7 - E_5) - I_5E_1 + I_7E_1] \quad (11)$$

$$T_{12} = \frac{3}{2\omega_r}[-I_5E_7 - I_7E_5] \quad (12)$$

To determine the amplitude of current harmonics, the following matrix equation must be solved by equating by equating T_0 to the reference torque T_e^* (output of speed controller) and setting T_6 and T_{12} to zero:

$$\begin{bmatrix} E_1 & E_5 & E_7 \\ E_7\_E_5 & -E_1 & E_1 \\ 0 & -E_7 & -E_5 \end{bmatrix} \times \begin{bmatrix} I_1 \\ I_5 \\ I_7 \end{bmatrix} = \frac{2\omega_r}{3} \begin{bmatrix} T_e^* \\ 0 \\ 0 \end{bmatrix} \quad (13)$$

As a result, the amplitudes of harmonic reference currents are determined as follows:

$$\begin{bmatrix} I_1^* \\ I_5^* \\ I_7^* \end{bmatrix} = \begin{bmatrix} 1.006 \\ -0.0671 \\ 0.0134 \end{bmatrix} \frac{2\omega_r T_e^*}{3} \quad (14)$$

Note, the reference value of the third harmonic current is set to zero because this harmonic does not contribute to torque generation.

3.2 MFPCSC method based on ultra-local model

An ultra-local model of a single-input, single-output system using only the system's input and output while disregarding mathematical model can be expressed as [23].

$$\dot{y} = \alpha u + F \quad (15)$$

where, y is output of the system, u is input of the system, F is sum of known and unknown disturbances of system as extended state, and α is a scaling coefficient of the designed model. Considering y^* as the reference output value of the system, $\hat{F}$ as the estimated value of F, the control law of state feedback controller can be expressed as:

$$u = \frac{\dot{y}^* - \hat{F} + \xi}{\alpha} \quad (16)$$

here ξ is the control law and can be the output of controller such as proportional-integral (PI). If extended state F is estimated with high accuracy, so $\hat{F} \cong F$, from (15) and (16) it results

$$\dot{e} + \xi = 0 \quad (17)$$

where $e = y^* - y$ represents the output tracking error. Assuming that ξ, the output of the proportional controller, is in the form $\xi = k_p e$, the control law of the closed-loop nonlinear system is described as follows:

$$u = \frac{\dot{y}^* - \hat{F} + k_p e}{\alpha}$$
$$\dot{e} + k_p e = 0 \quad (18)$$

It is clear that the performance of controller depends on the proportional controller coefficient (k_p) and the accuracy of the estimation.

To develop the ultra-local mathematical model of the modular double-winding, twelve-phase PMSM in the stationary stator frame, the following steps are taken. By rewriting (1) and using (2) for a considered winding such as winding A_1 of phase A, it results:

$$v_{A_1} = R_s i_{A_1} + \frac{d}{dt}\psi_{A_1} + e_{A_1} \quad (19)$$

or

$$v_{A_1} = R_s i_{A_1} + L_s \frac{di_{A_1}}{dt} + \frac{d}{dt} \sum_{x_j = B_1 \ldots Z_2} M_{A_1 x_j} i_{x_j} + \omega_r \psi_{PM} \sin(\theta_r) \quad (20)$$

It is observed that, in (20), the voltage of winding A_1 depends on the currents of other windings. However, given the modular nature of the power and control system, their values are not available, and the induced voltage due to the currents of other windings can be considered the unmodeled dynamics of the winding A_1. Considering parameter variations, unknown disturbances, and unmodeled dynamics, the mathematical model of winding A_1 can be expressed as follows:

$$v_{A_1} = (R_s + \Delta R) i_{A_1} + (L_s + \Delta L) \frac{di_{A_1}}{dt} + \omega_r (\psi_{PM} + \Delta \psi_{PM}) \sin(\theta_r) + f_{A_1} \quad (21)$$

that, ΔR, ΔL, and ψ_{PM} represent the resistance, inductance and permanent magnet flux variations of each phase, and f_{A1} indicates the unknown disturbances and unmodeled dynamics in phase A_1. Equation (21) can be rewritten as follows:

$$\frac{di_{A_1}}{dt} = \frac{v_{A_1}}{L_s} + \left(-\frac{(R_s + \Delta R) i_{A_1}}{L_s} - \frac{\Delta L}{L_s} \frac{di_{A_1}}{dt} - \frac{\omega_r (\psi_{PM} + \Delta \psi_{PM}) \sin(\theta_r)}{L_s} - \frac{f_{A_1}}{L_s} \right) \quad (22)$$

If the currents of each of the 24 windings of the motor are considered the system outputs, the applied voltages to the motor windings are considered the system inputs, and the other terms are considered the sum of the known and unknown disturbances of the system. Based on (15), the ultra-local mathematical model for winding A_1 PMSM can be expressed as follows:

$$\frac{di_{A_1}}{dt} = \alpha v_{A_1} + F_{A_1} \quad (23)$$

where α is the controller coefficient equal to the inverse of phase inductance ($\alpha = 1/\boldsymbol{L_s}$), and the sum of the disturbances for winding $\boldsymbol{A_1}$ is as follows:

$$F_{A_1} = -\frac{(R_s + \Delta R) i_{A_1}}{L_s} - \frac{\Delta L}{L_s} \frac{di_{A_1}}{dt} - \frac{\omega_r (\psi_{PM} + \Delta \psi_{PM}) \sin(\theta_r)}{L_s} - \frac{f_{A_1}}{L_s} \quad (24)$$

For other windings, the ultra-local mathematical model can also be presented in the same manner. In the next section, an ESO is designed for each winding to estimate the sum of the disturbances F_{A_1}.

3.3 Design of extended state observer (ESO)

Based on the ultra-local model given by (23), a linear extended state observer can be designed, with the state variables estimating the values of i_{A1} and F_{A1}. This observer can be designed using the feedback of the estimation error of the current i_{A1} as follows [30, 29]:

$$\begin{cases} e = x_1 - i_{A_1} \\ \dot{x}_1 = x_2 + \alpha v_{A_1} - \beta_1 \times e \\ \dot{x}_2 = -\beta_2 \times e \end{cases} \quad (25)$$

where $x_1 = \hat{\imath}_{A_1}$ ،$x_2 = \hat{F}_{A_1}$ are the state variables of the observer, those are the estimated values i_{A1} and F_{A1} respectively. β_1 and β_2 are the feedback gains of the observer's error, which influence the estimation quality and must be appropriately determined. To design the observer and determine the appropriate values for β_1 and β_1, the state-space representation of the linear ESO can be expressed as follows:

$$\begin{cases} \dot{x} = Ax + B v_{A_1} + D(y - \hat{y}) \\ \hat{y} = Cx \end{cases} \quad (26)$$

that $\hat{\boldsymbol{y}}$ is the estimated output y, and the vector x and observer matrices are as follows:

$$x = \begin{bmatrix} x_1 \\ x_2 \end{bmatrix}, A = \begin{bmatrix} 0 & 1 \\ 0 & 0 \end{bmatrix}, B = \begin{bmatrix} \alpha \\ 0 \end{bmatrix}, C^T = \begin{bmatrix} 1 \\ 0 \end{bmatrix}, D = \begin{bmatrix} \beta_1 \\ \beta_2 \end{bmatrix} \quad (27)$$

The characteristic equation of the ESO observer is expressed as follows:

$$|sI - (A - DC)| = s^2 + \beta_1 s + \beta_2 \quad (28)$$

For stability of the ESO, the roots of the (30) must be located in the left half of the complex plane. Hence, the following conditions must be met:

$$\begin{cases} \beta_1 = 2\omega_0 \\ \beta_2 = \omega_0^2 \end{cases} \quad (29)$$

The bandwidth $\boldsymbol{\omega_0}$ of the ESO determines the stability and dynamic performance of the observer. For PMSM drives, the current control loop (inner loop) typically requires a high bandwidth to meet dynamic response requirements.

3.4 Current regulation using current ESOs

The relationship between voltage and current for each winding of the motor follows a first-order ultra-local model such (26). Using the Euler discretization approximation, the voltage of motor winding A_1 can be calculated as follows:

$$v_{A_1}(k) = \frac{i_{A_1}(k+1) - i_{A_1}(k)}{\alpha T_s} - \frac{\hat{F}_{A_1}(k)}{\alpha} \quad (30)$$

where F_{A_1} is replaced by $\hat{F}_{A_1}$, that is determined by the ESO. By substituting $i_{A_1}(k+1)$ with the reference current of the phase A winding, i.e., i_A^* determined by (15), the reference voltage value of the motor winding A_1 is obtained as follows:

$$v_{A_1}^*(k) = \frac{i_A^*(k) - i_{A_1}(k)}{\alpha T_s} - \frac{\hat{F}_{A_1}(k)}{\alpha} \tag{31}$$

By modulating this voltage vector using fixed switching frequency modulation methods such as space vector modulation (SVM) or sinusoidal modulation, the switching signals for each H-bridge inverter shown in Fig. 4 are determined.

3.5 Speed control using speed ESO

In the continuation of the work, the speed control loop is implemented as model-free predictive control and it is augmented to proposed MFPCC method in previous section. The dynamic equation of the speed of PMSM from (4) can be rewritten as:

$$\frac{d\omega_m}{dt} = \frac{1}{J}(T_e - B\omega_m - T_L) \tag{32}$$

Considering ω_m as the output and T_e as the input of the model, (32) can be rewritten as same as (15) and (16) as follows:

$$\frac{d\omega_m}{dt} = \beta T_e + F_m \tag{33}$$

$$F_m = \frac{1}{J}(-B\omega_m - T_L) \tag{34}$$

where F_m shows the total mechanical disturbances of the system and $\beta = 1/J$ is the input gain. It is possible to repeat the process similar to (17) to estimate $\hat{F}_m$ where $x = \omega_m$ is the state variable of the mechanical part of the system.

$$\begin{aligned} \dot{h}_m &= -l(\omega_m)h_m - l(\omega_m)\left[\lambda(\omega_m) + \beta i_q\right] \\ \hat{F}_m &= h_m + \lambda(\omega_m) \\ \lambda(\omega_m) &= \ell\omega_m \\ l(\omega_m) &= \frac{\partial\lambda(\omega_m)}{\partial\omega_m} = \ell \end{aligned} \tag{35}$$

Using Euler's approximation, (35) can be rewritten as follows:

$$\frac{\omega_m(k+1) - \omega_m(k)}{T_s} = \beta T_e(k) + \hat{F}_m(k) \tag{36}$$

Considering $\omega_m(k+1) = \omega_m^*$, the reference value of torque T_e can be calculated as follows:

$$T_e^* = T_e(k+1) = \frac{\omega_m^* - \omega_m(k)}{\beta T_s} - \frac{\hat{F}_m(k)}{\beta} \tag{37}$$

Fig. 5 shows the block diagram of a twelve-phase PMSM motor control system using a harmonic current injection strategy, with current and speed control implemented via ESO (Extended State Observer) observers.

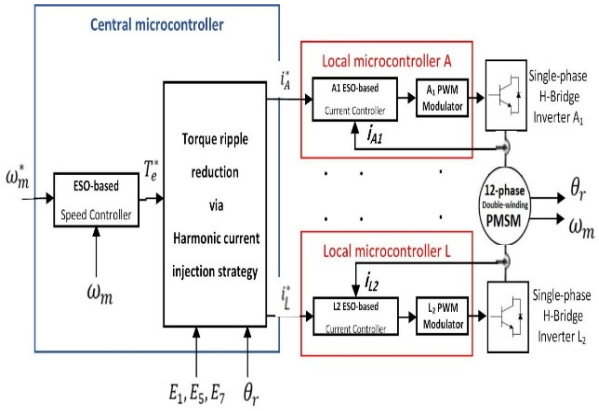

Fig 5. Block diagram MFPCSC method for the twelve-phase with double windings using Extended Space Observers

4 Fault-tolerant control in a modular twelve-phase PMSM drive

Significant research has been conducted over the past two decades on fault-tolerant control for multi-phase PMSM motors with fewer than 12 phases, including 5-phase and 6-phase asymmetric configurations [25-26]. However, limited studies have addressed 12-phase brushless permanent magnet motors (PMSM/BLDC). For instance, [27] proposes a fault-tolerant control strategy for a 12-phase PMSM motor in a flywheel application, treating the motor as four independent three-phase groups (each modeled in the *dq* frame and powered by separate three-level inverters) to handle single open-phase faults. This approach was later extended in [28] to accommodate two-phase open-circuit faults across different three-phase groups.

The proposed method in this work relies on balancing the second harmonic torque components of the motor windings under fault conditions. In healthy operation, these harmonic components cancel each other, resulting in a ripple-free instantaneous torque (assuming ideal sinusoidal back-EMF). However, when one or more phases are lost, this balance is disrupted, introducing torque oscillations at twice the rotor frequency. To restore equilibrium, the compensation strategy adjusts the current angles of the remaining healthy phases. For example, if the fundamental harmonic vectors of the 12 phases are represented as in Fig. 6(a), their second harmonic torque components form a balanced system, as illustrated in Fig. 6(b). By dynamically modifying the phase angles of healthy windings, the sum of these harmonics can be driven back to zero, mitigating torque ripple under fault conditions.

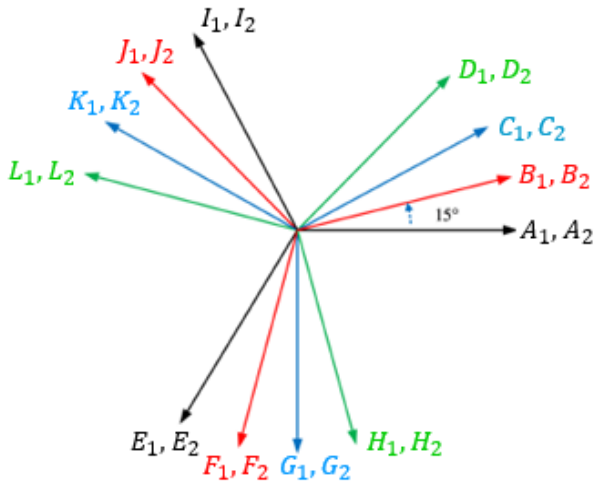

(a) First order harmonic vectors of phases currents

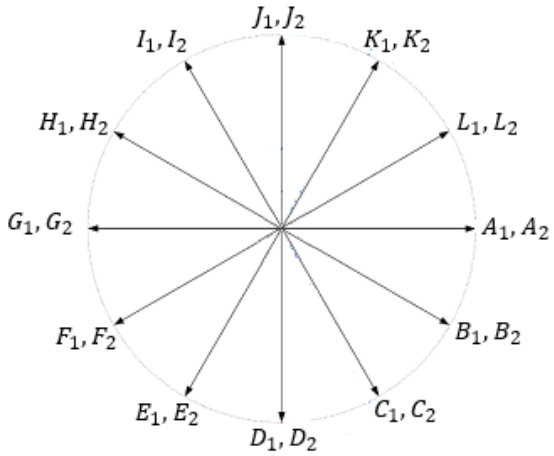

(b) Second order harmonic vectors of torques

Fig 6. Diagram of current and second order harmonic vectors in the 12-phase PMSM

4.1 One-phase open-circuit failure

In the motor's healthy state, the second harmonic of torque can be analyzed by dividing the twelve windings (in one half) into four three-phase groups, as illustrated in Fig. 6(b). For instance, consider the three-phase group $A_1I_1E_1$, where the resultant second harmonic torque is zero under normal conditions. However, if winding A_1 becomes open-circuit, the remaining windings (E_1 and I_1) effectively form an unbalanced two-phase system. This imbalance generates a second harmonic torque component. To mitigate the resulting torque ripple, the proposed Fault-Tolerant Control (FTC) strategy compensates for the second harmonic torque, as depicted in Fig. 7. When an open-circuit fault occurs, the healthy phase currents are symmetrically adjusted in magnitude and phase to compensate for the lost phase. The key objective is to ensure that the vector sum of the second harmonic torques from the remaining windings cancels out. For example, in the case of the $A_1I_1E_1$ group:

- The vectors I_1 and E_1 can be shifted by $\theta_{shift} = 30^o$ toward the lost winding A_1, resulting in new positions I'_1 and E'_1.
- Alternatively, other *compensation* schemes are possible, such as shifting only E_1 by 60° or only I_1 by -60°, as long as the resultant second harmonic torque of the group sums to zero.

Since the torque angle of each phase is determined by both the current angle and the back-EMF voltage angle (which is fixed), the required phase shift must be applied to the current angle of the compensating windings. Additionally, the current magnitudes of I'_1 and E'_1 must be adjusted accordingly to ensure effective cancellation of the second harmonic torque. This approach ensures minimal torque ripple while maintaining motor performance under fault conditions.

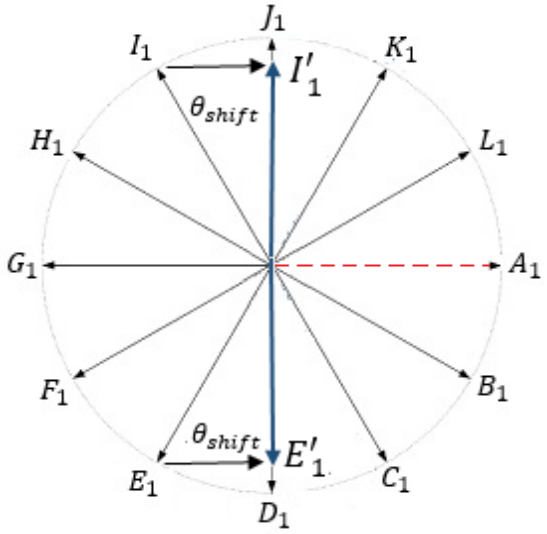

Fig 7. Diagram of the second-order harmonic torque for the proposed fault-tolerant control method under single-phase open-circuit failure

As a general rule for compensation, when using only one healthy phase for compensation, the current angle of the preceding phase (in positive sequence) to the faulty phase should be shifted by 60°. There are 12 possible cases of single-phase open-circuit faults within half of the stator circumference, as detailed in Table 1. If the fault occurs in the second winding of a phase (e.g., A_2), the same compensation method applies. Considering all single-winding fault possibilities across the entire motor, there are 24 possible cases of single-winding faults.

Table 1. One-phase failure and corresponding compensator phases

Faulty winding	3-phase group	Compensator winding		Shift angle in winding	
A_1	$A_1I_1E_1$	I_1	E_1	-30^o	$+30^o$
B_1	$B_1J_1F_1$	F_1		$+60^o$	
C_1	$C_1K_1G_1$	G_1		$+60^o$	
D_1	$D_1L_1H_1$	H_1		$+60^o$	
E_1	$A_1I_1E_1$	I_1		$+60^o$	
F_1	$B_1J_1F_1$	J_1		$+60^o$	
G_1	$C_1K_1G_1$	K_1		$+60^o$	
H_1	$D_1L_1H_1$	L_1		$+60^o$	
I_1	$A_1I_1E_1$	A_1		$+60^o$	
J_1	$B_1J_1F_1$	B_1		$+60^o$	
K_1	$C_1K_1G_1$	C_1		$+60^o$	
L_1	$D_1L_1H_1$	D_1		$+60^o$	

4.2 Two-phases open-circuit failure

This failure can occur in two cases: (1) Two faulty phases in separate three-phase groups, such as A_1 and B_1 . (2) Both faulty phases in the same three-phase group, such as A_1 and I_1. In case (1) as shown in Fig. 8(a), when the faulty phases are in different groups, two three-phase groups $C_1K_1G_1$ and $D_1L_1H_1$ remain balanced, producing no second-order harmonic torque. However, the other two groups $A_1I_1E_1$ and $B_1J_1F_1$ operate as unbalanced two-phase PMSMs, generating torque ripple with a second-order harmonic. The fault-tolerant control method mentioned in the previous section can be applied separately to both groups $A_1E_1I_1$ and $B_1J_1F_1$. Specifically, the vectors E_1 and I_1 can be shifted by 30° toward the faulty winding A_1 and the vector F_1 can be shifted by +60° so that it aligns opposite to J_1.

In case (2), that both faulty phases are in the same group, If the windings A_1 and I_1 were lost, the remaining phase E_1 in the same group generates second-order harmonic torque ripple. The only solution is to use its opposite vector K_2, located in the other half of the stator circumference. However, K_2 belongs to the $C_2K_2G_2$ group and contributes to torque production. To mitigate torque ripple, the magnitude of K_2 should be doubled, provided it does not exceed the current limit. Totally, there are 66 possible two-phase fault states in each half of the stator circumference. Some of these cases are summarized in Table 2.

4.3 Three-phases open-circuit failure

This failure can be occurred in three cases: (1) Three faulty phases to be in three separate three-phase groups such as A_1,, B_1 and C_1 or, case (2);

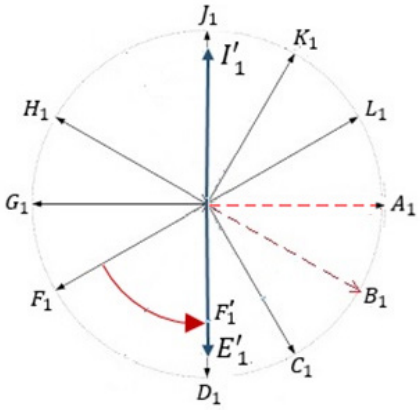

(a) Two faulty phases ($\boldsymbol{A_1}$, $\boldsymbol{B_1}$) belong to separate three-phase groups

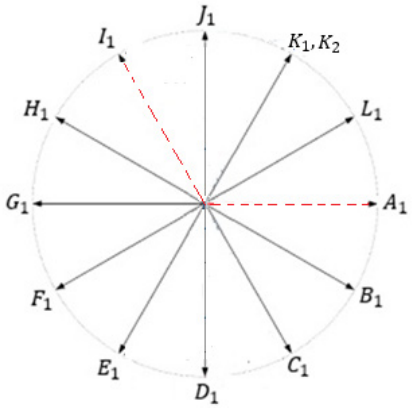

(b) Two faulty phases ($\boldsymbol{A_1}$, $\boldsymbol{I_1}$) belong to one three-phase group

Fig 8. Diagram of second-order harmonic torque for proposed fault-tolerant control method in case of two-phase failure

Table 2. Selected examples of two-phase failures along with their corresponding compensator phases (66 fault cases)

Faulty windings	Compensator windings			Shift angle in windings		
A_1 , B_1	I_1	E_1	F_1	-30^o	$+30^o$	$+60^o$
A_1 , C_1	I_1	E_1	G_1	-30^o	$+30^o$	$+60^o$
A_1 , D_1	I_1	E_1	H_1	-30^o	$+30^o$	$+60^o$
A_1 , E_1	I_1	E_1	C_2	-30^o	$+30^o$	0^o
A_1 , F_1	I_1	E_1	J_1	-30^o	$+30^o$	$+60^o$
A_1 , G_1	I_1	E_1	K_1	-30^o	$+30^o$	$+60^o$
A_1 , H_1	I_1	E_1	L_1	-30^o	$+30^o$	$+60^o$
A_1 , I_1	I_1	E_1	K_2	-30^o	$+30^o$	0^o
A_1 , J_1	I_1	E_1	B_1	-30^o	$+30^o$	$+60^o$
A_1 , K_1	I_1	E_1	C_1	-30^o	$+30^o$	$+60^o$
A_1 , L_1	I_1	E_1	D_1	-30^o	$+30^o$	$+60^o$

Two faulty phases to be in one three-phase group such A_1 and I_1 and the third faulty phase such D_1 to be in

another group, and case (3); three faulty phases such A_1, I_1, E_1 are belonged in one three-phase group.

In the first case, the proposed FTC for one-phase failure in section 4.1 can be employed for each faulty-phase. In the second case, the proposed FTC for one-phase and two-phases failure in sections 4.1 and 4.2 are used. For the third case, there is no need for compensation. There are 220 three-phase fault cases in each half of the stator circumference in general, that some of them are summarized in table 3.

Table 3. Some examples of three-phase failure and corresponding compensator phases (220 fault cases)

Faulty windings	Compensator windings	Shift angle in windings
A_1, B_1, C_1	$(I_1,E_1),(F_1),(G_1)$	$(-30^o, +30^o), (+60^o), (+60^o)$
A_1, C_1, D_1	$(E_1),(G_1),(H_1)$	$(+60^o), (+60^o), (+60^o)$
A_1, I_1, D_1	$(K_{2)}, (H_1)$	$(0^o), (+60^o)$
A_1, E_1, D_1	$(C_{2)}, (H_1)$	$(0^o), (+60^o)$
A_1, I_1, E_1	–	No need for compensation
B_1, J_1, F_1	–	No need for compensation
C_1, K_1, G_1	–	No need for compensation
D_1, L_1, H_1	–	No need for compensation

4.4 Fault in four or more phases

This failure can occur in four cases:

- Case 1: Four faulty phases are distributed across separate three-phase groups, such as $A_{1,}, B_1, C_1$ and D_1.
- Case 2: Three faulty phases belong to one three-phase group (e.g., A_1, I_1 and E_1), while the fourth faulty phase (e.g., D_1) is in another group.
- Case 3: Two faulty phases (e.g., A_1, I_1) are in one three-phase group, and the other two faulty phases (e.g., B_1, C_1 to) are in different groups.
- Case 4: Two faulty phases (e.g., A_1, I_1) are in one three-phase group, and another two faulty phases (e.g., B_1, J_1) are in a different group.

For compensation in case 1, the proposed Fault-Tolerant Control (FTC) for one-phase failure (Section 4.1) can be applied separately to each faulty phase, following Table 1. In case 2, for the three faulty phases in one group, no compensation is needed. For the remaining faulty phase, the FTC from Section 4.1 is applied. In case 3, for the two faulty phases in the same group, the FTC from Section 4.2 is used. For the other two faulty phases, the FTC from Section 4.1 is applied, and for case 4, for both pairs of faulty phases in different groups, the FTC from Section 4.2 is implemented. In general, there are 495 possible four-phase fault combinations in each half of the stator circumference, some of which are summarized in Table 4.

4.5 Fault in more 5 phases

For failures involving five or more phases, the methods described in the previous sections (4.1–4.3) can be applied, considering the distribution of faulty phases across the four three-phase groups.

Table 4. Some examples of four-phase failure and corresponding compensator phases (495 fault cases)

Faulty windings	Compensator windings	Shift angle in windings
A_1, B_1, C_1, D_1	$(E_1), (F_1), (G_1), (H_1)$	$(+60^o), (+60^o), (+60^o), (+60^o)$
A_1, I_1, E_1, D_1	(H_1)	$(+60^o)$
A_1, I_1, C_1, D_1	$(K_2),(G_1), (H_1)$	$(0^o), (+60^o), (+60^o)$
A_1, I_1, B_1, J_1	$(K_2),(L_2)$	$(0^o), (0^o)$

5 Simulation results

In this section, for a twelve-phase, 10-poles PMSM with rated specification of 200 kW, 2000 N.m, 400 V, 320 rpm, $R_s = 30\,m\Omega$, $L_s = 825\,mH$, $J = 0.3\,kg.m^2$, $\psi_{PM} = 1.5\,Wb$, $K_e = 1.1\,V/(\frac{rad}{\sec})$ is considered. The motor behavior is simulated using the harmonic current injection method with three current regulators: PI, hysteresis, and ESO-based. Figures 9 to 11 present the dynamic response of the twelve-phase PMSM drive, including the reference and actual speed, electromagnetic torque, and reference/actual phase currents for each regulator. In these simulations, the two windings of each phase are connected in series and powered by a single-phase H-bridge inverter.

The motor's non-sinusoidal back-EMF waveform introduces harmonics into the reference current. Simulation results demonstrate that all three regulators—PI, PR, and ESO—deliver effective current tracking performance. However, the ESO regulator outperforms the others, yielding the lowest torque ripple.

A detailed comparison of the regulators' performance is provided in Table 5, which summarizes the peak-to-peak current ripple and torque ripple for each controller. The data confirms that while all three achieve satisfactory current regulation, the ESO's advanced harmonic compensation capability results in significantly smoother torque output.

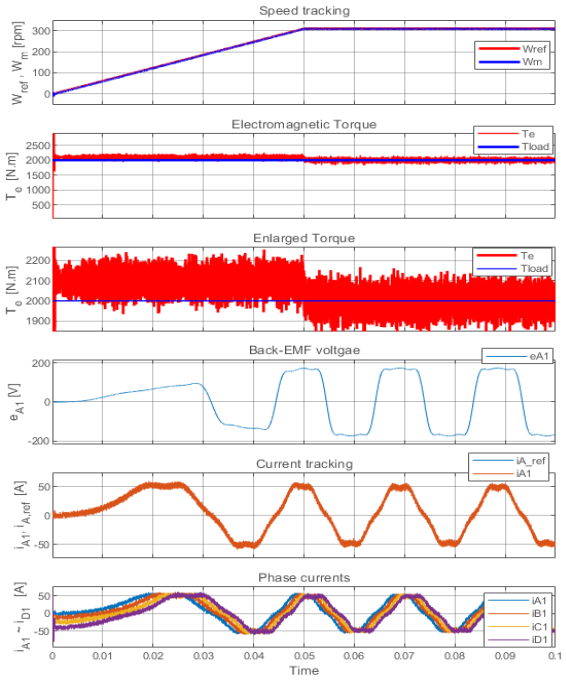

Fig 9. Dynamic response of 12-phase PMSM drive using PI current regulators

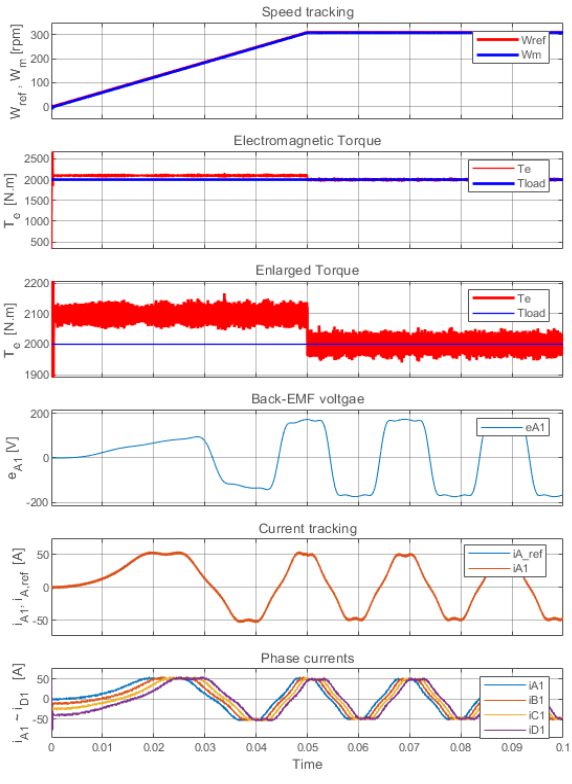

Fig 10. Dynamic response of 12-phase PMSM drive using hysteresis current regulators

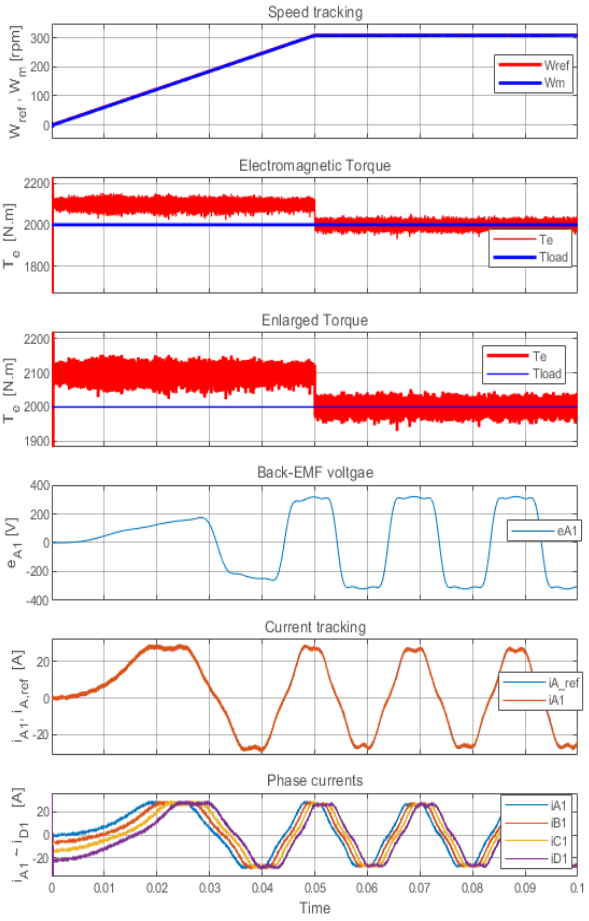

Fig 11. Dynamic response of 12-phase PMSM drive using ESO-based controllers

Table 5. Comparison of various current regulators on torque ripple

Current ripple (A)	Torque ripple (N.m)	Current regulator
12	240	PI
3	60	Hysteresis with band 1 A
1.2	24	MFPCSC+NDOs

To simulate the performance of the single-phase fault tolerant control system, it is assumed that the winding A_1 of the phase A is lost at time $t = 0.65\ sec$. Fig. 12 shows the simulation of the system performance. To observe the disturbance in the generated torque, it is assumed that the fault-tolerant control (FTC) algorithm is activated with $0.2\ sec$ delay at time $t = 0.85\ sec$, and on this way, the angle of the two windings E_1 and I_1 are shifted by $+30^o$ and -30^o respectively according to Table 1. The magnitude of current is determined via speed controller, that has risen after compensation from 81 A to 123 A. The motor torque fluctuates slightly due to the large number of healthy phases in the motor.

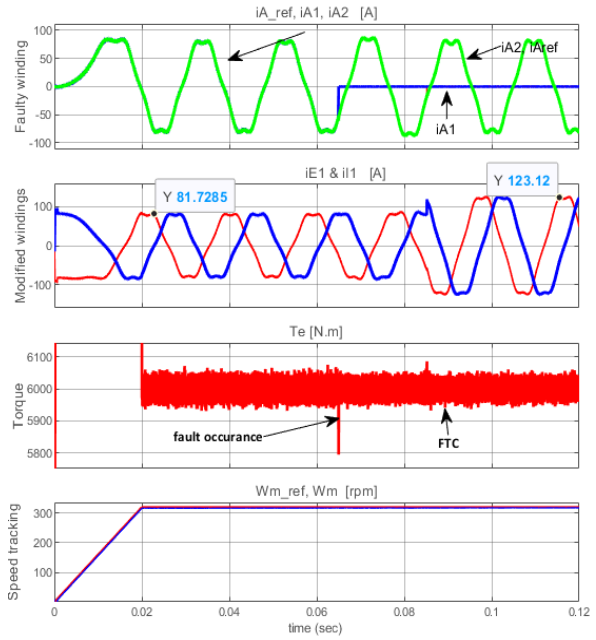

Fig 12. Dynamic response of proposed FTC under one-phase failure $(\boldsymbol{A_1})$

Fig. 13 shows the simulation of the system performance under the condition of a fault in two phases. Two windings A_1 and B_1 are lost at time $t = 0.65\ sec$ and to reduce torque ripple, according to row 1 of table 2, the current angle of the three windings (E_1, F_1, I_1) is changed by $(30^o, +60^o, -30^o)$. The current magnitude is also increased almost 50% via command of speed controller. When a fault occurs, the torque undergoes a slight fluctuation, and after applying the fault-tolerant control method at time $0.65\ sec$, the second-order harmonic of torque ripple disappeared.

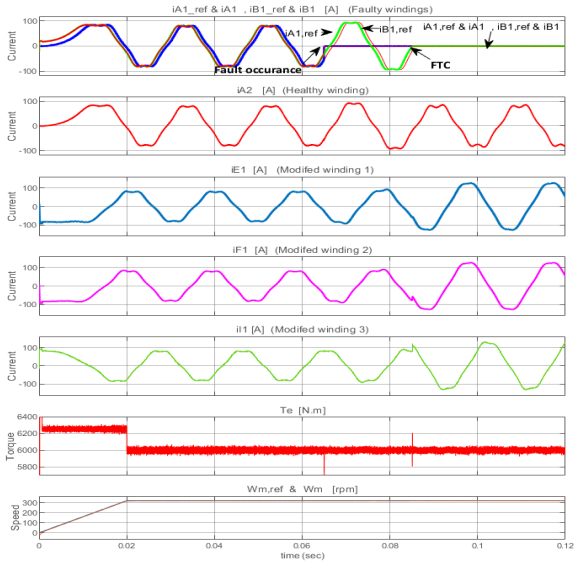

Fig 13. Dynamic response of proposed FTC under two-phases failure $(\boldsymbol{A_1}, \boldsymbol{B_1})$

Fig. 14 shows the simulation of the system performance under a load torque of 6000 N.m under three-phase on-circuit failure. The three windings (A_1, B_1, C_1) are lost at time $t = 0.65\ sec$. When a fault occurs, the torque undergoes a severe fluctuation, and even the speed drops from rpm 316 to rpm 260. To compensate the torque ripple, according to row 1 of table 3, the current angle of the four windings (I_1, E_1, F_1, K_1) are changed by $(-30^o, +30^o, +60^o, -60^o)$. After applying the FTC method at time $0.85\ sec$, the torque and speed return to their previous state. The magnitude of the currents is increased almost 50% and reaches from 80 A to 126 A.

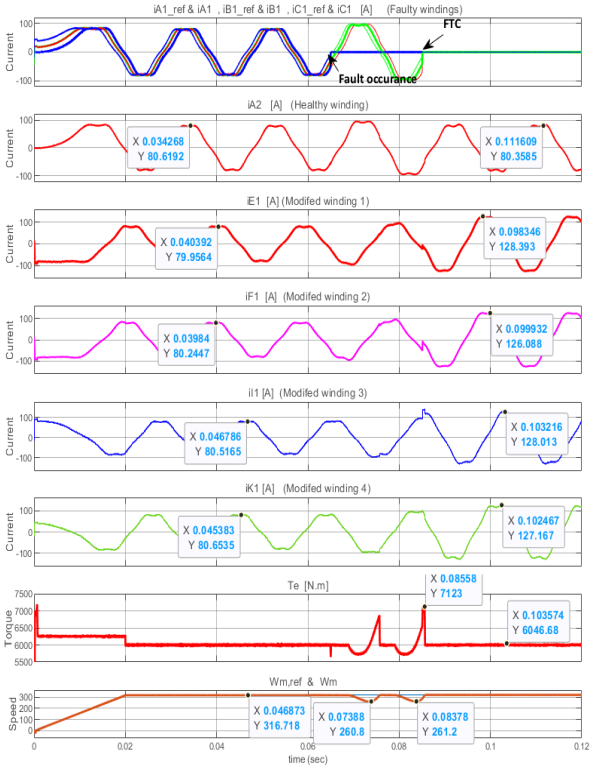

Fig 14. Dynamic response of proposed FTC under three-phases failure $(\boldsymbol{A_1}, \boldsymbol{B_1}, \boldsymbol{C_1})$

Fig. 15 also shows the dynamic performance of the proposed FTC while four-phase open-circuit fault occurs. under a constant load torque of 6000 N.m, four windings (A_1, B_1, C_1, D_1) are lost at time $t = 0.65\ sec$. After failure, as shown, the torque decreases sharply and the speed also drops significantly and is going to be unstable. To prevent the instability of the drive, FTC is applied at time $0.85\ sec$ and the current angle of the four windings (I_1, E_1, G_1, H_1) are changed by $(-30^o, +30^o, +60^o, +60^o)$ as mentioned in table 4. The magnitude of the healthy currents is increased almost 50% and reaches from 80 A to 126 A.

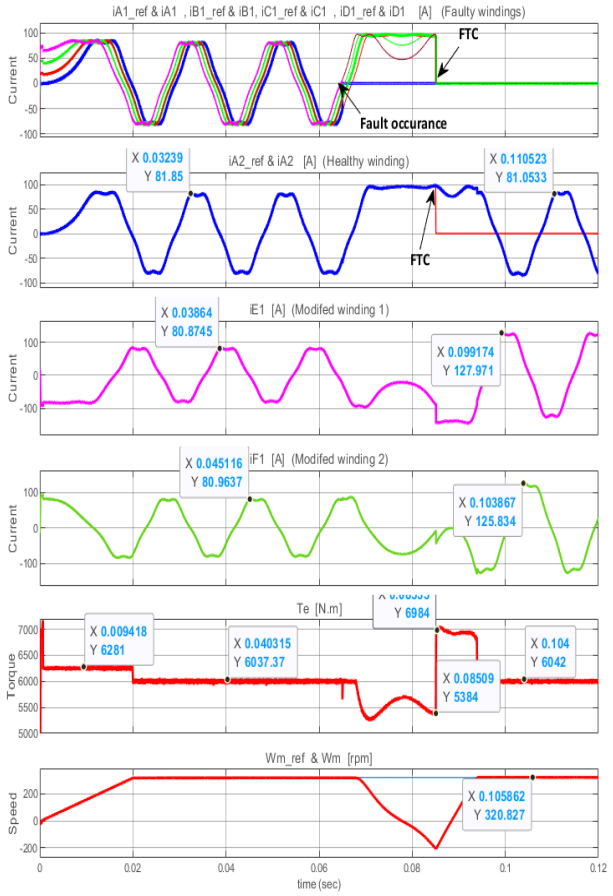

Fig 15. Dynamic response of proposed FTC under four-phases failure ($\boldsymbol{A_1, B_1, C_1, D_1}$)

6 Conclusion

This paper investigates the control of a modular twelve-phase non-sinusoidal PMSM with double stator windings. Given the independent control of each phase, the motor is modeled in a 12-axis stationary reference frame. To enhance motor performance and mitigate torque ripple induced by back-EMF harmonics, a harmonic current injection method is implemented. For accurate tracking of harmonic reference currents, a model-free predictive control strategy is employed, utilizing current and speed extended state observers (ESOs). Under normal operating conditions, the proposed method ensures robust dynamic performance in the modular drive, requiring only prior knowledge of the back-EMF harmonic content. The drive's performance is further analyzed under various fault scenarios, with a fault-tolerant control (FTC) strategy proposed for each case. This strategy focuses on balancing the second-order harmonic torque in the remaining windings. Notably, while the proposed FTC effectively eliminates the second-order torque harmonic arising from the fundamental components of current and back-EMF, neither this method nor existing approaches can fully suppress higher-order torque harmonics caused by current and back-EMF harmonics. An additional critical consideration is that the loss of one or more windings reduces the motor's torque capacity. Under a constant load torque exceeding the motor's maximum producible torque (determined by the remaining phases' current limits), instability occurs. However, if the load torque follows a propeller-type characteristic (e.g., proportional to the square of speed), the motor can continue operating at a reduced speed, as the output torque adjusts to match the load torque. Simulation results validate the effectiveness of the proposed modeling and control methods for this modular motor drive.

References

[1] J.S. Thongam, M. Tarbouchi, A.F. Okou, D. Bouchard, R. Beguenane, "Trends in naval ship propulsion drive motor technology", IEEE Electrical Power & Energy Conf., 2013.

[2] D.S. Kanturska, "Features in the selection and operation of AC motors for electric propulsion system in ship", 15th International Conference on Electrical Machines, Drives and Power Systems (ELMA), 2017.

[3] B. Chen, J. Lv, X. Jiang, "Simplified Model Predictive Control of a Twelve-Phase Permanent Magnet Synchronous Motor", 45th Annual Conference of the IEEE Industrial Electronics Society (IECON), vol. 1, 2019.

[4] Y. Mingqing, M. Hongwei, R. Jingpan, "Research on Control Strategy of Diode Clamped Three-Level 12-Phase Permanent Magnet Synchronous Motor", Chinese Automation Congress (CAC), pp. 3352-3357, 2020.

[5] Z. Wangguang, D. Wang, Y. Wang, Y. Li, "A review on fault-tolerant control of PMSM", Chinese Automation Congress (CAC), pp. 3854-3859, 2017.

[6] Y.S. Jeong, S.K. Sul, S.E. Schulz, "Fault detection and fault-tolerant control of interior permanent-magnet motor drive system for electric vehicle", IEEE Trans. on Industry Applications, vol. 41, no. 1, pp. 46-51, 2005.

[7] F. Barrero, M.J. Duran, "Recent Advances in the Design, Modeling, and Control of Multiphase Machines—Part I", IEEE Trans. on Industrial Electronics, vol. 63, no. 1, pp. 449-458, 2016.

[8] S. Kallio, M. Andriollo, A. Tortella, J. Karttunen, "Decoupled d-q Model of Double-Star Interior-Permanent-Magnet Synchronous Machines", IEEE Trans. on Industrial Electronics, vol. 60, no. 6, pp. 2486-2494, 2013.

[9] Y. Hu, Z.Q. Zhu, M. Odavic, "Comparison of Two-Individual Current Control and Vector Space

Decomposition Control for Dual Three-Phase PMSM", IEEE Trans. on Industry Application, vol. 53, no. 5, pp. 4483-4492, 2017.

[10] L.R. Rocha, E.C. Silva, P.H.A. Silva, G.X. Prestes, B.C.R. Cordeiro, L.F. Pessoa, R.P. Vieira, "Evaluation Methodology of Current Control Techniques for Torque Ripple Reduction in Non-Sinusoidal PMSM", IEEE 8th Southern Power Electronics Conference (SPEC), 2023.

[11] M.J. Nam, J.H. Kim, K.Y. Cho, H.W. Kim, Y. Cho, "Torque Ripple Reduction of an Interior PM Synchronous Motor by Compensating Harmonic Currents Based on Flux Linkage Harmonics", Journal of Power Electronics, vol. 17, no. 5, pp. 1223-1230, 2017.

[12] S. Mu, J. Kang, Z. Zhong, Z. Ma, "Improved detecting method for multiple rotating reference frames based harmonic control of PMSMs", Chinese Automation Congress (CAC), pp. 5458-5463, pp. 2020.

[13] J. Taylor, D.F. Valencia Garcia, W. Taha, M. Mohamadian, "Dynamic Modelling of Multiphase Machines Based on the VSD Transformation," SAE Technical Paper 2021-01-0774, doi:10.4271/2021-01-0774, 2021.

[14] A. Halvaei Niasar, M. Ahmadi, S.H. Edjtahed, "Sensorless Control of Non-Sinusoidal Permanent Magnet Brushless Motor Using Selective Torque Harmonic Elimination Control Method Based on Full-Order Sliding Mode Observer", Advances in Power Electronics Journal, vol. 2016, no. 9358604, pp. 1-13, 2016.

[15] M.Z. Choudri, R.W. De Doncker, R. Loewenherz, N.H. Fuengwarodsakul, "Concept for Distributed Field Oriented Control of Twelve-Phase Permanent Magnet Machine", IEEE International Conference on Power, Energy and Innovations (ICPEI), 2022.

[16] Y. Du, W. Song, G. Yao, L. Zhou, "A Harmonic Current Suppression Method based on Repetitive Control for Twelve-phase PMSM", IEEE 2nd China International Youth Conference on Electrical Engineering (CIYCEE), 2021

[17] J. Zhu, J. Yuan, Z. Nie, J. Xu, X. Zeng, "Research on Dual 12-Phase 12-Slot Winding Permanent-Magnet Propulsion System Based on All-SiC Power Module", IEEE Trans. on Industry Applications, Vol. 58, No. 6, pp. 7692-7700, 2022.

[18] B. Chen, J. Lv, X. Jiang, "A Sensorless Control Method based on MRAS for 12-Phase PMSM in FESS", IEEE 10th International Symposium on Power Electronics for Distributed Generation Systems (PEDG), pp. 1055-1059, 2019.

[19] Q. Liu, K. Hameyer, "Torque ripple minimization for direct torque control of PMSM with modified FCSMPC", IEEE Trans. on Industry Applications, vol. 52, no. 6, pp. 4855– 4864, 2016.

[20] S. Chai, L. Wang, E. Rogers, "A cascade MPC control structure for a PMSM with speed ripple minimization", IEEE Trans. on Industrial Electronics, vol. 60, no. 8, pp. 2978– 2987, 2012.

[21] Y. Zhou, H. Li, H. Yao, "Model-free control of surface mounted PMSM drive system", IEEE Int. Conf. Industrial Technology (ICIT), pp. 175–180, 2016.

[22] J. Han, "From PID to active disturbance rejection control", IEEE Trans. on Industrial Electronics, vol. 56, no. 3, pp. 900–906, 2009.

[23] Z. Sun, Y. Deng, J. Wang, Z. Wei, H. Cao, "Finite Control Set Model-Free Predictive Current Control of PMSM With Two Voltage Vectors Based on Ultralocal Model", IEEE Trans. on Power Electronics, vol. 38, no. 1, pp. 776 – 788, 2023.

[24] G. Feng, C. Lai, M. Kelly, C. Kar, "Dual Three-Phase PMSM Torque Modeling and Maximum Torque per Peak Current Control Through Optimized Harmonic Current Injection", IEEE Trans. on Industrial Electronics, vol. 66, no. 5, pp. 3356-3368, 2019.

[25] H. Wang, W. Zhao, H. Tang, T. Tao, "Improved Fault-Tolerant Model Predictive Torque Control of Five-Phase PMSM by Using Deadbeat Solution", IEEE Trans. on Energy Conversion, vol. 37, no. 1, pp. 210-218, 2022.

[26] P.F.C. Gonçalves, S.M.A Cruz, "Fault-Tolerant Predictive Current Control of Six-Phase PMSMs with Minimal Reconfiguration Requirements", IEEE Journal of Emerging and Selected Topics in Power Electronics, 2022.

[27] W. Li, J. Lv, X. Jiang, X. Zhang, S. Sheng, "A Fault-Tolerant Control Method of 12-Phase PMSM in FESS", IEEE 10th International Symposium on Power Electronics for Distributed Generation Systems (PEDG), 2019.

[28] J. Lv, G. Tian, X. Jiang, "Fault-Tolerant Control of Twelve-Phase PMSM Based on Motor Model Reconstruction in FESS", IEEE 4th Conference on Energy Internet and Energy System Integration (EI2), 2020 .

Davood Maleki, was born in 1980 in Malayer, Iran. He received a Bachelor's degree in Electronics and a Master's degree in Electrical Machines from Malek Ashtar Industrial University in Shahin Shahr, Isfahan. His Bachelor's thesis was on the design of a buck-boost regulator for a 400 to 24 converter, and His Master's thesis focused on the construction of an LSPMSM drive. He is currently a PhD student at University of Kashan.

His interests are control and implementation of multi-phase PMSM drives.

Abolfazl Halvaei Niasar (S'04–M'06–SM'14) was born in Kashan, Iran in 1974. He received his B.Sc., M.Sc., and Ph.D. in 1996, 1999, and 2008 from Isfahan University of Technology (IUT), University of Tehran (UT) and Iran University of Science and Technology (IUST) respectively, all in electrical engineering. He has joined the Department of Electrical and Computer Engineering at University of Kashan, Kashan, Iran since 2008 as assistant professor. He has authored more than 150 technical papers published in journals and conference proceedings. He is the holder of two Iranian patents and has directed some industrial research projects. His current major research interests include PM and brushless DC motor (BLDC) drives, sensorless drives, design, analysis and control of electrical machines. Dr. Halvaei is senior member of the Institute of Electrical and Electronics Engineers, IEEE.